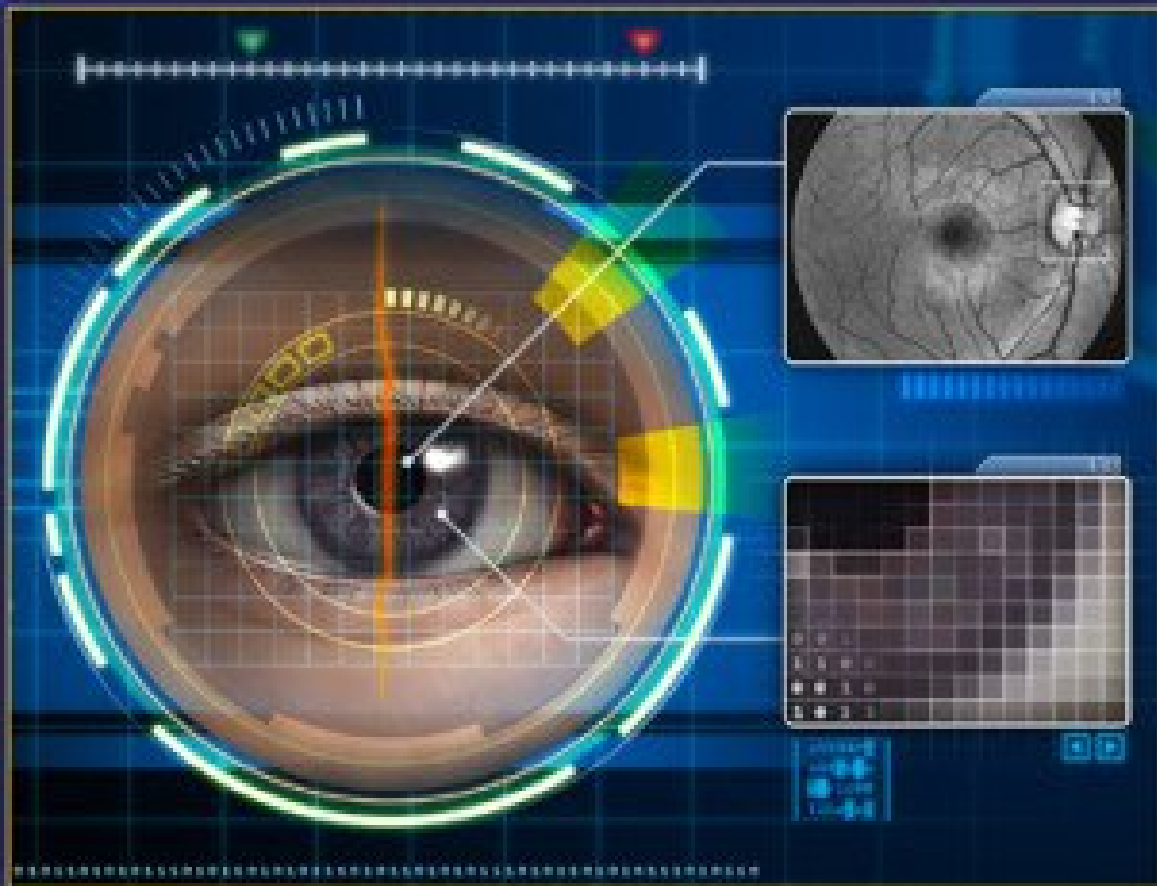


OPHTHALMOLOGY IMAGING AND APPLICATIONS



Edited by
E. Y. K. Ng
U. Rajendra Acharya
Rangaraj M. Rangayyan
Jasjit S. Suri

 CRC Press
Taylor & Francis Group

22

Effects of Electromagnetic Fields on Specific Absorption Rate and Heat Transfer in the Human Eye

Teerapot Wessapan and Phadungsak Rattanadecho

CONTENTS

22.1	Introduction	426
22.2	Problem Formulation	427
22.3	Mathematical Model Formulation.....	429
22.3.1	Electromagnetic Wave Propagation Equation	430
22.3.1.1	Boundary Condition for Wave Propagation Analysis	431
22.3.2	Heat Transfer Equation	433
22.3.2.1	Boundary Condition for Heat Transfer Analysis	434
22.3.3	Calculation Procedure.....	435
22.4	Results and Discussion	435
22.4.1	Verification of the Model	435
22.4.2	Electric Field Distribution.....	436
22.4.2.1	Effect of Power Density on Electric Field Distribution.....	436
22.4.3	SAR Distribution.....	438
22.4.3.1	Effect of Power Density on SAR Distribution.....	438
22.4.4	Temperature Distribution.....	439
22.4.4.1	Effect of Heat Transfer Model on Temperature Distribution	439
22.4.4.2	Effect of Power Density on Temperature Distribution	441
22.4.5	Concluding Remarks.....	443
References.....		444

Nomenclature

C	Specific heat capacity (J/(kg K))
E	Electric field intensity (V/m)
e	The tear evaporation heat loss (W/m ²)
f	Frequency of incident wave (Hz)
H	Magnetic field (A/m)
h	Convection coefficient (W/(m ² K))
j	Current density (A/m ²)
k	Thermal conductivity (W/(m K))
n	Normal vector
p	Pressure (N/m ²)
Q	Heat source (W/m ³)

T	Temperature (K)
u	Velocity (m/s)
t	Time

Greek Letters

β	Volume expansion coefficient (1/K)
μ	Magnetic permeability (H/m)
ϵ	Permittivity (F/m)
σ	Electric conductivity (S/m)
ω	Angular frequency (rad/s)
ρ	Density (kg/m ³)
ω_b	Blood perfusion rate (1/s)
Γ	External surface area

Subscripts

am	Ambient
b	Blood
ext	External
i	Subdomain
met	Metabolic
r	Relative
ref	Reference
0	Free space, initial condition

22.1 Introduction

AQ1 The electromagnetic (EM) waves of the different power levels and frequencies penetrate deep into the human body causing health risks. In recent years, there has been some increasing public concern with the interaction between the human body and the EM fields. Since the eye is one of the most sensitive organs to the EM fields, the high-intensity EM fields may lead to a variety of ocular effects. However, the resulting thermophysiological response of the eye to EM fields is not well understood. Therefore, it is important to investigate the ocular effects occurred during exposure to EM fields. Although the safety standards written in terms of maximum tissue specific absorption rate (SAR) values are regulated, they are not stated in terms of maximum temperature increase in the eye caused by EM energy absorption. The eye temperature increasing gradually can cause serious long-term effects on eyesight and vision. There have been medical case reports of cataract formation in humans via microwave radiation [1]. It is reported that a temperature increase in the eye of 3°C–5°C leads to induce cataract formation [2] and a temperature above 41°C is necessary for production of posterior lens opacities [3]. Therefore, to gain insight into the phenomenon of eye temperature distribution induced by EM fields, it is necessary to have a detailed knowledge of the absorbed power distribution and the temperature distribution.

AQ2 Previous studies focused on the effects of EM fields on the human eye [4,5]. Nevertheless, their analysis has been conducted based on the maximum SAR values permitted by public safety standards regulation [6,7]. For example, in studies of an interaction between the EM fields and the human eye, most of them have mainly focused on SAR and have not considered the heat transfer. Consequently, it could not be fully understood. In addition, there

have been few experimental data on the correlation of SAR levels with the temperature increase in the human tissue. Therefore, a modeling of heat transport is needed to completely explain the actual process of interaction between the EM fields and the human eye.

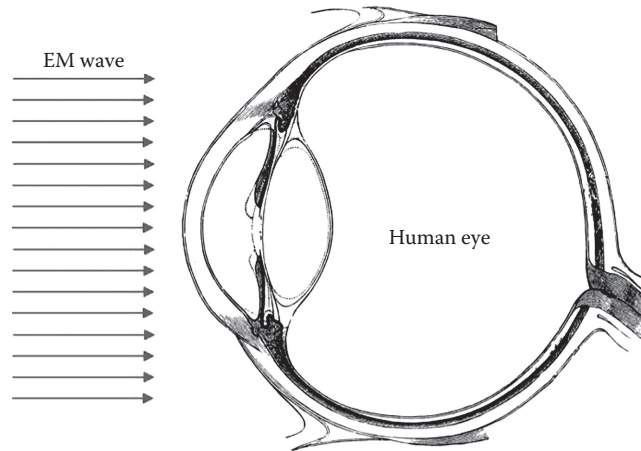
Thermal modeling of human tissue is important as a tool to explore the effects of external heat sources and investigate abnormalities in the tissue. Recently, the modeling of heat transport in human tissue has been considered by many researchers [8–20]. Most studies of heat transfer analysis in the human eye used heat conduction equation [8–14]. Some studies carried out on natural convection in human eye based on heat conduction model [15,16]. Ooi and Ng [16,17] studied the effect of aqueous humor (AH) hydrodynamics on the heat transfer in the eye based on heat conduction model. Meanwhile, the Pennes' bioheat equation [18,19], based on the heat diffusion equation for a blood-perfused tissue, is used for modeling of heat transfer in the human eye as well [20,21]. Ooi and Ng also developed a 3D model of the human eye [22], extending their 2D model [21]. Recently, researchers have used the porous media models to investigate the transport phenomena in biological media instead of a simplified bioheat model [23–25]. Shafahi and Vafai [26] proposed the porous media along with natural convection model to analyze the eye thermal characteristics during exposure to thermal disturbances. Narasimhan and Vishnampet [27] proposed the porous medium model of the sclera and the choroid to study the effect of choroidal blood flow on transscleral drug delivery to the retina. Many researchers have been tried to conduct the advanced model using the coupled model of heat and laser irradiation in the human eye [28–30]. Results from similar models of Ooi et al. [30] for various applications were also presented in continuation [31–34].

Although the porous media and natural convection models of the human eye have been used in the previous biomedical studies [15–16,26,27], most studies of the human eye exposed to EM fields have not been considering the porous media approach, and natural convection approach is sparse or nonexistent. Wessapan and Rattanadecho [35] investigated the SAR and temperature distributions of EM fields in the eye using porous media theory. There are few studies on an interaction between the temperature and the EM fields in realistic physical model of the human organs especially the eye due to its complexity. Therefore, to provide information on exposure levels and health effects from EM fields, it is necessary to simulate both of the EM fields and the heat transfer, based on porous media theory within an anatomical model particularly the eye.

In this study, a 2D eye model was exploited to simulate the SAR and temperature distributions. EM wave propagation in the eye was investigated by using Maxwell's equations. An analysis of heat transfer in the eye exposed to a transverse magnetic (TM) mode of EM fields was investigated using a developed heat transfer model (included the conduction and natural convection heat transfer mode), which was proposed by Shafahi and Vafai [26]. The SAR and the temperature distribution in various parts of the human eye during exposure to EM fields at 900 MHz, which are obtained by numerical solution of EM wave propagation and heat transfer equation, are presented. This book chapter was based on empirical data from the work of Wessapan and Rattanadecho [35], with permission from ASME.

22.2 Problem Formulation

In fact, the human exposures to EM radiation have increased exponentially. The human eye is exposed daily to radiation from sources such as mobile phones, microwave oven,



AQ3 **FIGURE 22.1**
EM fields from an EM radiation device.

monitors, and wireless networks and other EM fields commonly found in our daily life. It is known that the human eye is one of the most sensitive organs to EM radiation. This is because the crystalline lens and the cornea are nonvascular tissue with low metabolism and the eye has no thermal sensors and protective reflexes. An investigation of the human eye exposure to EM fields can be done with difficulty due to the eye's complex geometry and its being a heterogeneous tissue. Moreover, this investigation cannot be done by experiments due to the ethical considerations. Exposing a human to EM fields for experimental purposes is still restricted. It is more convenient and ethical to develop a realistic human eye model through numerical simulation. Figure 22.1 shows radiation of EM fields from an EM radiation device to the human body. These EM fields fall on the human eye that causes heating in the deeper tissue, which leads to tissue damage and cataract formation.

Our first step in the evaluation of the effects of a certain exposure to EM fields in the eye is to determine the induced internal EM fields and their spatial distributions. Thereafter, with the EM energy absorption resulting in an increased temperature in the eye, other interactions could be then considered. This study considers the coupling between the EM and heat transfer equations to model the distribution of temperature fields induced by EM radiation in the eye.

In this study, the eye model, which is based on a physical model we developed in the previous research [26], comprises seven types of tissue including posterior chamber, anterior chamber, cornea, iris, sclera, lens, and vitreous. Different types of tissue have different dielectric and thermal properties. In the sclera layer, there are two more layers known as choroid and retina that are relatively thin compared to the size of the sclera itself. To simplify the problem, these layers are assumed to be homogeneous. The iris and the sclera, which have the same properties, are modeled together as one homogenous region [16]. Figure 22.2 shows the 2D eye model used in this study [35]. The dielectric [36,37] and thermal properties [16] of tissue are shown in Tables 22.1 and 22.2, respectively. Each tissue is assumed to be homogeneous and electrically as well as thermally isotropic.

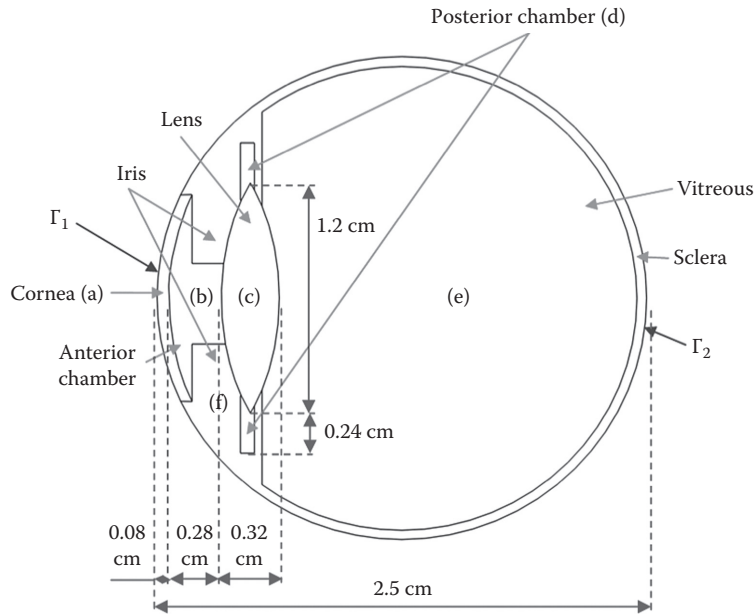


FIGURE 22.2 Human eye vertical cross section. (From Wessapan, T. and Rattanadecho, P., *ASME Trans. J. Heat Transfer*, 134, 091101, 2012. With permission.)

TABLE 22.1
Dielectric Properties of Tissues at 900 and 1800 MHz

Tissue	Frequency 900 MHz		Frequency 1800 MHz	
	ϵ_r	σ (S/m)	ϵ_r	σ (S/m)
Cornea (a)	52.0	1.85	55.0	2.32
Anterior chamber (b)	73.0	1.97	75.0	2.40
Lens (c)	51.3	0.89	41.1	1.29
Posterior chamber (d)	73.0	1.97	75.0	2.40
Vitreous (e)	74.3	1.97	73.7	2.33
Sclera (f)	52.1	1.22	52.7	1.68
Iris (f)	52.1	1.22	52.7	1.68

Source: Wessapan, T. and Rattanadecho, P., *ASME Trans. J. Heat Transfer*, 134, 091101, 2012. With permission.

22.3 Mathematical Model Formulation

The intensity of the internal fields in the body depends on various parameters such as an operating frequency, the power intensity, a mode of propagation, the body geometry, the tissue dielectric properties, a distance from EM source, and the presence of other objects in the body vicinity. When the EM waves pass from one medium to another, they can be absorbed, reflected, refracted, or transmitted, depending on the dielectric property of the

TABLE 22.2

Thermal Properties of Human Eyes

Tissue	ρ (kg/m ³)	k (W/m °C)	C_p (J/kg °C)	μ (N s/m ²)	β (1/K)
Cornea (a)	1050	0.58	4178	—	—
Anterior chamber (b)	996	0.58	3997	0.00074	0.000337
Lens (c)	1000	0.4	3000	—	—
Posterior chamber (d)	996	0.58	3997	—	—
Vitreous (e)	1100	0.603	4178	—	—
Sclera (f)	1050	1.0042	3180	—	—
Iris (f)	1050	1.0042	3180	—	—

Source: Wessapan, T. and Rattanadecho, P., *ASME Trans. J. Heat Transfer*, 134, 091101, 2012. With permission.

exposed body and the operating frequency of the EM source. Most of the absorbed EM energies are converted into heat.

22.3.1 Electromagnetic Wave Propagation Equation

EM waves are a phenomenon in the form of self-propagating waves in a free space or in matter. EM waves consist of electric and magnetic fields oscillating in phase perpendicular to each other and to the direction of wave propagation. Maxwell's equations for electric and magnetic fields are used to investigate EM wave propagation in different media and radiation. An EM wave propagating in a linear, isotropic, homogeneous medium can basically be described by Maxwell's equations:

$$\nabla \times \bar{E} = -\frac{\partial \bar{B}}{\partial t} \quad (22.1)$$

$$\nabla \times \bar{B} = \frac{1}{c^2} \frac{\partial \bar{E}}{\partial t} \quad (22.2)$$

$$\nabla \cdot \bar{E} = 0 \quad (22.3)$$

$$\nabla \cdot \bar{B} = 0 \quad (22.4)$$

where

\bar{E} is the electric field intensity (V/m)

\bar{B} is the magnetic flux density (Wb/m² or T)

c is the light velocity in the medium (m/s)

$c_0 = 2.99792458 \times 10^8$ is the speed of light in free space

$$c = \frac{c_0}{n} \quad (22.5)$$

where n is the refractive index of the medium, $n = \sqrt{\epsilon_r}$ and ϵ_r is the relative dielectric constant.

Maxwell's equations for free space are expressed by

$$\nabla \times \bar{E} = j\omega B \quad (22.6)$$

$$\nabla \times \bar{B} = \frac{-1}{c^2} j\omega \bar{E} \quad (22.7)$$

$$\nabla \cdot \bar{E} = 0 \quad (22.8)$$

$$\nabla \cdot \bar{B} = 0 \quad (22.9)$$

where

ω is the angular frequency (rad/s)

$$j = \sqrt{-1}$$

The general form of Maxwell's equations is simplified to demonstrate the EM fields penetrated in the eye as the following equation:

$$\nabla \times \left(\left(\epsilon_r - \frac{j\sigma}{\omega\epsilon_0} \right)^{-1} \nabla \times H_z \right) - \mu_r k_0^2 H_z = 0 \quad (22.10)$$

where

H is the magnetic field (A/m)

μ_r is the relative magnetic permeability

ϵ_r is the relative dielectric constant

$\epsilon_0 = 8.8542 \times 10^{-12}$ F/m is the free space permittivity

k_0 is the free space wave number (1/m)

22.3.1.1 Boundary Condition for Wave Propagation Analysis

This study investigated ocular changes during exposure to EM radiation with a particular power density. A schematic description of a boundary condition is shown in Figure 22.3: the uniform wave flux falls on the left side of the eye. Therefore, for the left boundary, an EM simulator uses a TM wave propagation port with a specified power density:

$$S = \frac{\int (E - E_1) \cdot E_1}{\int E_1 \cdot E_1} \quad (22.11)$$

Boundary conditions along the interfaces between different mediums are considered as continuity boundary conditions:

$$n \times (E_1 - E_2) = 0. \quad (22.12)$$

The outer side of the calculated domain, that is, free space, is considered as a scattering boundary condition:

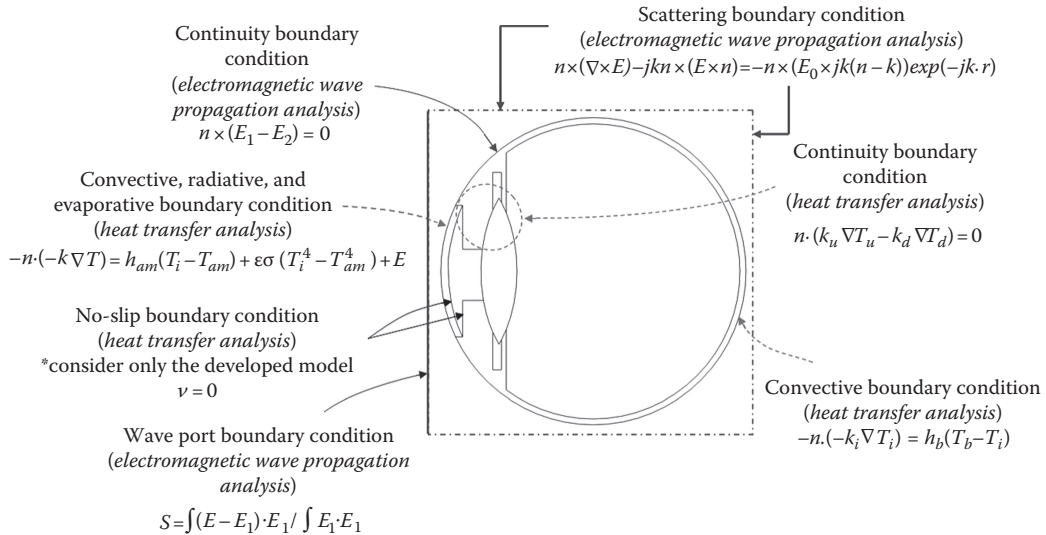


FIGURE 22.3 Boundary condition for the analysis of EM wave propagation and heat transfer. (From Wessapan, T. and Rattanadecho, P., *ASME Trans. J. Heat Transfer*, 134, 091101, 2012. With permission.)

$$n \times (\nabla \times E_z) - jkE_z = -jk(1 - k \cdot n)E_{0z} \exp(-jk \cdot r) \tag{22.13}$$

where

- AQ4 k is the wave number (m^{-1})
- σ is the electric conductivity (S/m)
- n is the normal vector
- $j = \sqrt{-1}$
- E_0 is the incident plane wave (V/m)

Microwave EM exposure levels are expressed in terms of power density (in W/m^2 or W/ft^2).

- AQ5 However, for microwave band, both the electric field intensity (in V/m) and the magnetic field intensity (in A/m) are used to represent the fields. According to the International Commission of Non-Ionizing Radiation Protection (ICNIRP) guidelines [6], an average SAR (in W/kg) (or whole-body average SAR) is defined as the ratio of the total absorbed power in the exposed body to its mass where the local SAR refers to the absorbed energy value per unit volume or mass, which can be arbitrarily small. The SAR is defined as

$$SAR = \frac{\sigma}{2\rho} |E|^2 \tag{22.14}$$

where

- AQ6 σ is the electric conductivity (S/m)
- ρ is the tissue density (kg/m^3)
- \bar{E}_i is the electric field intensity (V/m)

The SAR can also be determined from the increase in tissue temperature over a short period of time following the exposure as

$$\frac{\Delta T}{\Delta t} = \frac{\text{SAR}}{C} \quad (22.15)$$

where

- ΔT is the temperature increase
- Δt is the exposure duration
- C is the specific heat

22.3.2 Heat Transfer Equation

From a macroscopic point of view, thermal effects resulting from the EM waves' absorption inside the biological tissue are expressed in terms of the bioheat equation [18,19] based on the heat diffusion equation, which can be written as

$$\rho C \frac{\partial T}{\partial t} = \nabla \cdot (k \nabla T) + \rho_b C_b \omega_b (T_b - T) + Q_{met} + Q_{ext} \quad (22.16)$$

where

- ρ is the tissue density (kg/m^3)
- C is the tissue heat capacity ($\text{J}/(\text{kg K})$)
- k is the tissue thermal conductivity ($\text{W}/(\text{m K})$)
- T is the tissue temperature ($^{\circ}\text{C}$)
- T_b is the blood temperature ($^{\circ}\text{C}$)
- ρ_b is the blood density (kg/m^3)
- C_b is the blood heat capacity
- ω_b is the blood perfusion rate ($1/\text{s}$)
- Q_{met} is the metabolism heat source (W/m^3)
- Q_{ext} is the external heat source (EM heat source density) (W/m^3)

$$Q_{ext} = \frac{\sigma}{2} |E|^2 \quad (22.17)$$

This study utilized two pertinent thermal models to investigate the heat transfer behavior of the eye when exposed to the EM fields.

Model I: Conventional heat transfer model [21]

This model assumes the metabolic heat generation and the blood perfusion in the eye to be zero. The governing equation therefore looked just like the classical heat conduction equation:

$$\rho_i C_i \frac{\partial T_i}{\partial t} = \nabla \cdot (k_i \nabla T_i) + Q_{ext}; \quad i = a, b, c, d, e, f \quad (22.18)$$

where

- i denotes each subdomain in the eye model as shown in Figure 22.2
- ρ is the tissue density (kg/m^3)
- C is the tissue heat capacity ($\text{J}/(\text{kg K})$)
- k is the tissue thermal conductivity ($\text{W}/(\text{m K})$)
- T is the tissue temperature (K)
- t is the time

Model II: Developed heat transfer model [26]

In this model, the fluid motion is considered only inside the anterior chamber [16]. There is a blood flow in the iris/sclera part, by which the blood flow plays a role to adjust the temperature of the eye [26]. For the rest of the parts, the metabolic heat generation is neglected due to the fact that these parts comprise mainly water [16]. The governing equation for the flow of heat in cornea, posterior chamber, lens, and vitreous is the same as Equation 22.18.

This model accounts for the existence of AH in the anterior chamber. The heat transfer process consists of both conduction and natural convection, which can be expressed as follows:

Continuity equation

$$\nabla \cdot u_i = 0; \quad i = b \quad (22.19)$$

Momentum equation

$$\rho_i \frac{\partial u_i}{\partial t} + \rho_i u_i \nabla \cdot u_i = -\nabla p_i + \nabla \cdot [\mu(\nabla u_i + \nabla u_i^T)] + \rho_i g \beta_i (T_i - T_{ref}); \quad i = b \quad (22.20)$$

where

β is the volume expansion coefficient (1/K)

u is the velocity (m/s)

p is the pressure (N/m²)

μ is the dynamic viscosity of AH (N s/m²)

T_{ref} is the reference temperature that we consider here as 37°C

The effects of buoyancy due to the temperature gradient are modeled using the Boussinesq approximation, which states that the density changes to the temperature change and the pressure perturbations are negligible [16].

AQ7 The energy equation is expressed as follows:

$$\rho_i C_i \frac{\partial T_i}{\partial t} - \nabla \cdot (k_i \nabla T_i) = -\rho C_i v_i \cdot \nabla T_i + Q_{ext}; \quad i = b. \quad (22.21)$$

The sclera/iris is modeled as a porous medium with blood perfusion, by which the local thermal equilibrium is assumed between the blood and the tissue. A modified Pennes' bioheat equation [26,38] is used to calculate the temperature distribution in the sclera/iris tissue:

$$(1 - \varepsilon) \rho_i C_i \frac{\partial T_i}{\partial t} = \nabla \cdot ((1 - \varepsilon) k_i \nabla T_i) + \rho_b C_b \omega_b (T_b - T_i) + Q_{ext}; \quad i = f \quad (22.22)$$

where ε is the porosity.

22.3.2.1 Boundary Condition for Heat Transfer Analysis

The heat transfer analysis excluding the surrounding space is considered only in the eye. The cornea surface as shown in Figure 22.3 is considered as the convective, radiative, and evaporative boundary condition for all of the models:

$$-n \cdot (-k\nabla T) = h_{am}(T_i - T_{am}) + \varepsilon\sigma(T_i^4 - T_{am}^4) + e \quad \text{on } \Gamma_1 \quad i = a \quad (22.23)$$

where

- Γ_i is the external surface area corresponding to section i
- e is the tear evaporation heat loss (W/m²)
- T_{am} is the ambient temperature (K)
- h_{am} is the convection coefficient (W/(m² K))

The blood temperature generally assumed to be the same as the body's core temperature causes heat to be transferred into the eye [16]. The surface of the sclera is assumed to be a convective boundary condition for all of the models:

$$-n \cdot (-k_i\nabla T_i) = h_b(T_b - T_i) \quad \text{on } \Gamma_2 \quad i = f \quad (22.24)$$

where

- h_b is the convection coefficient of blood
- Γ_1 and Γ_2 are the corneal surface and the sclera surface of the eye, respectively.

22.3.3 Calculation Procedure

The computational scheme used in this study is applied to assemble a finite element model and compute a local heat generation. The EM calculation is carried out by using tissue properties. To obtain a good approximation, a fine mesh is specified in the sensitive areas, by which a variable mesh method for solving the problem is proposed as in Figure 22.4. The governing equations with initial and boundary conditions are then solved. The 2D model with triangular elements is used to discretize the domain, and the Lagrange quadratic is then used to approximate temperature and SAR variation across each element. To reduce the global mesh size, a mesh convergence test was performed. The mesh with approximately 10,000 elements is obtained.

22.4 Results and Discussion

In this analysis, the effect of power density (5, 10, 50, and 100 mW/cm²) on distributions of SAR and temperature profiles in the eye is systematically investigated using two models: the conventional heat transfer model and the developed heat transfer model. The models of the EM and thermal fields are solved numerically. The dielectric and thermal properties as in Tables 22.1 and 22.2, respectively, are used for the simulation. In this study, we follow the guidelines of the ICNIRP, the radiated power used at the maximum SAR value of 2 W/kg (general public exposure) and 10 W/kg (occupational exposure) [6].

22.4.1 Verification of the Model

In order to verify the accuracy of the present numerical models, the simulated results from this study are validated against the numerical results obtained by Shafahi and Vafai [26] who studied the same geometric model as this. Moreover, the numerical results are then

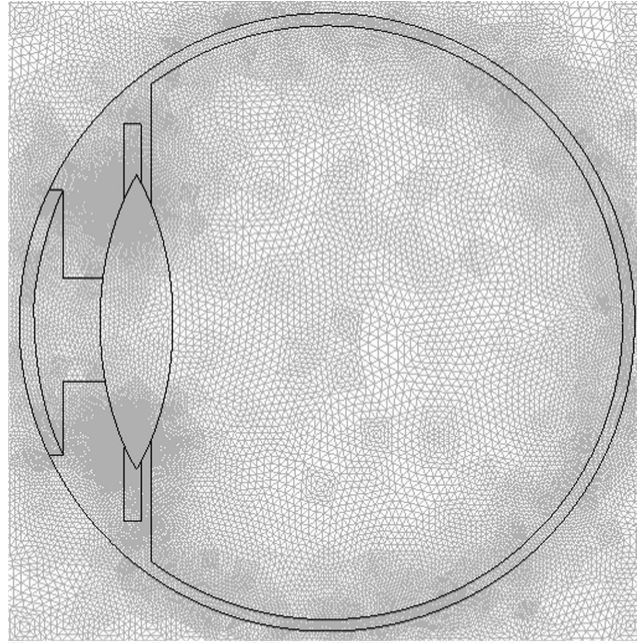


FIGURE 22.4
A 2D finite element mesh of human eye model.

compared to the experimental results of the rabbit obtained from Legendijk [8]. The validation case assumes that the rabbit body temperature is 38.8°C , the tear evaporation heat loss is 40 W/m^2 , the ambient temperature is 25°C , and the convection coefficient of ambient air is $20\text{ W/(m}^2\text{ K)}$. The results of the selected test case are presented in Figure 22.5 for the temperature distribution in the eye. Figure 22.5 clearly shows a good agreement of the temperature distribution in the eye between the present solution and that of Shafahi and Vafai [26] and Legendijk [8]. In the figure, the simulated results of the conventional heat transfer model and the developed heat transfer model provides a good agreement with the simulated results obtained from Shafahi and Vafai [26]. This favorable comparison provides confidence in the results of the present numerical model.

22.4.2 Electric Field Distribution

To illustrate the penetrated electric field distribution inside the eye, the predicted results obtained from our proposed models are required.

22.4.2.1 Effect of Power Density on Electric Field Distribution

Due to the different dielectric characteristics of the various tissue layers, a different fraction of the supplied EM energy will become absorbed in each layer in the eye. Consequently, the reflection and transmission components at each layer contribute to the resonance of standing wave in the eye. Figure 22.6 shows the simulation of an electric field pattern inside the eye exposed to EM field in TM mode operating at the frequency of 900 MHz propagating along the vertical cross section of the eye model, by which the varying power densities are done. As is obvious from Figure 22.6, the higher values of the electric fields in

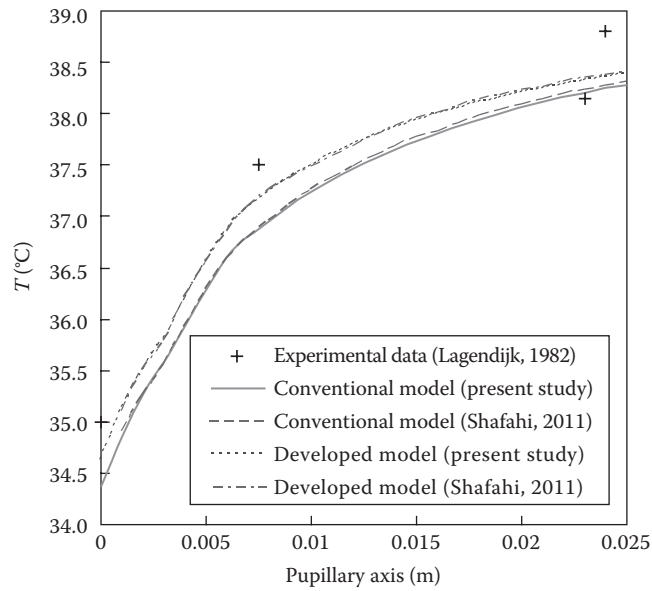


FIGURE 22.5 Comparison of the calculated temperature distribution to the temperature distribution obtained by Shafahi and Vafai and the Lagendijk’s experimental data; $h_{am} = 20 \text{ W}/(\text{m}^2 \text{ K})$ and $T_{am} = 25^\circ\text{C}$. (From Wessapan, T. and Rattanadecho, P., *ASME Trans. J. Heat Transfer*, 134, 091101, 2012. With permission.)

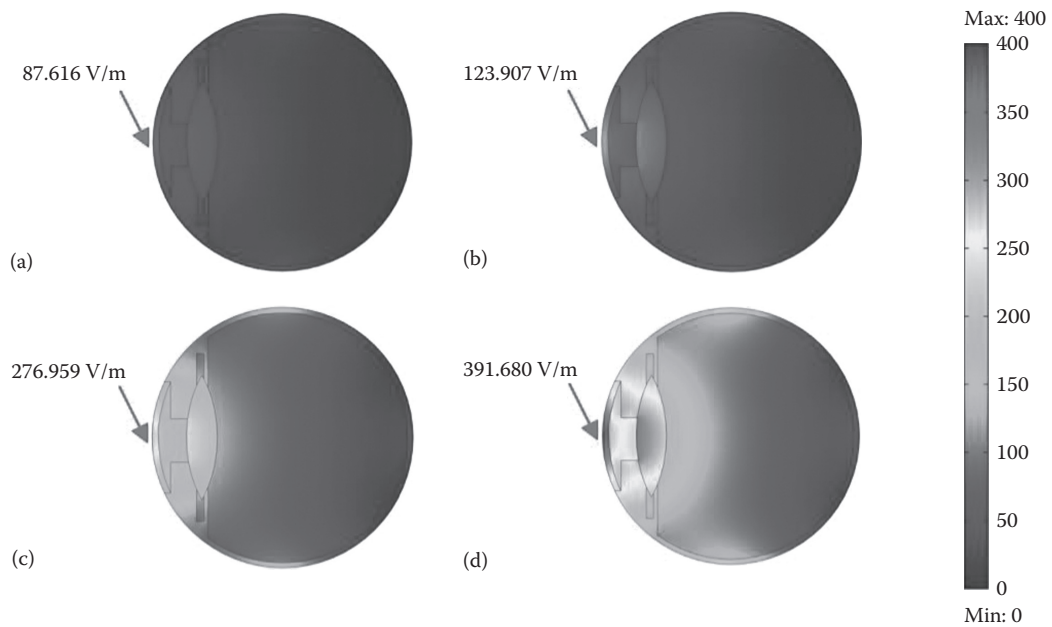


FIGURE 22.6 Electric field distribution (V/m) in human eye exposed to the EM frequency of 900 MHz at the power densities of (a) $5 \text{ mW}/\text{cm}^2$, (b) $10 \text{ mW}/\text{cm}^2$, (c) $50 \text{ mW}/\text{cm}^2$, and (d) $100 \text{ mW}/\text{cm}^2$. (From Wessapan, T. and Rattanadecho, P., *ASME Trans. J. Heat Transfer*, 134, 091101, 2012. With permission.)

AQ8 all cases occur in the outer part area of the eye, especially in the cornea and lens. The three highest electric field intensity values in the eye at all power densities occur in the cornea, lens, and iris, respectively. This is because the lower value of their dielectric properties (ϵ_r) shown in Table 22.1 corresponds to Equation 22.10, as well as these tissues are located close to the exposed surface, by which it causes the EM fields to penetrate easily into these tissues. The electric fields deep inside the eye are extinguished where the electric field attenuates due to the absorbed EM energy and the electric fields are then converted to heat. Moreover, the electric field distribution also showed a strong dependence on the dielectric properties of the tissue. Certainly, the maximum electric field intensity at the higher power density is greater than that of the lower power density. The maximum electric field intensities are 391.680, 276.959, 123.907, and 87.616 V/m at the power densities of 100, 50, 10, and 5 mW/cm², respectively.

22.4.3 SAR Distribution

22.4.3.1 Effect of Power Density on SAR Distribution

AQ9 For the SAR distribution in the eye, we found that the amplitude corresponds to the electric fields. Figure 22.7 shows the SAR distribution evaluated on the vertical cross section of the eye exposed to the EM frequency of 900 MHz at various power densities. The results of the SAR values in the eye are evident from Figure 22.7. The SAR values are increased corresponding to the electric field intensities (Figure 22.6). The maximum SAR values are 135.15, 67.575, 13.525, and 6.763 W/kg at the power densities of 100, 50, 10, and 5 mW/cm², respectively. Comparing to the maximum SAR value of 2 W/kg (general public exposure)

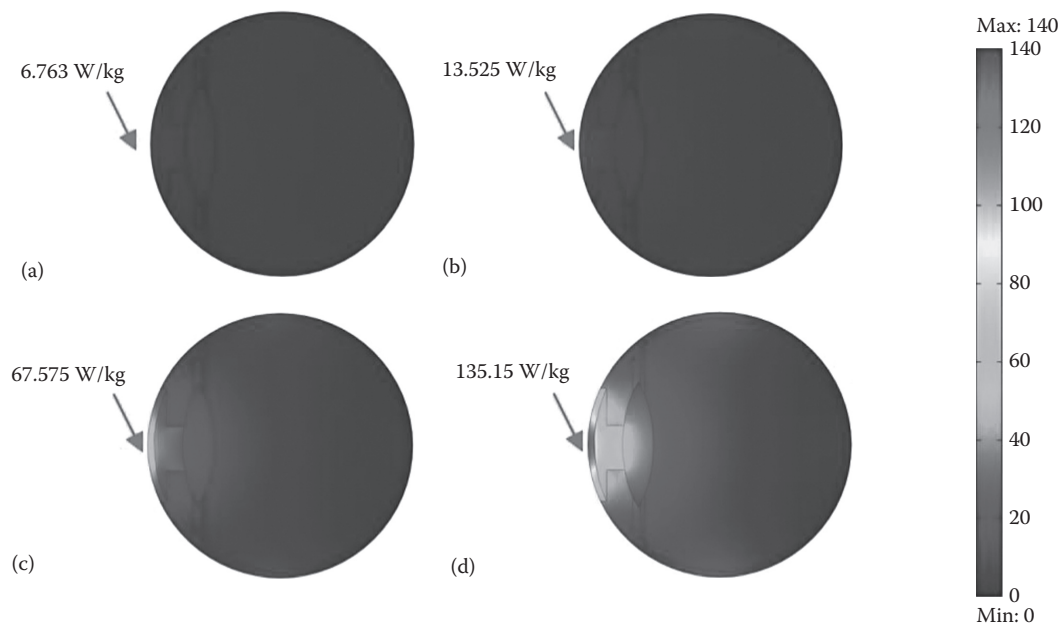


FIGURE 22.7

SAR distribution (W/kg) in human eye exposed to the EM frequency of 900 MHz at the power densities of (a) 5 mW/cm², (b) 10 mW/cm², (c) 50 mW/cm², and (d) 100 mW/cm². (From Wessapan, T. and Rattanadecho, P., *ASME Trans. J. Heat Transfer*, 134, 091101, 2012. With permission.)

and 10 W/kg (occupational exposure) [6], the resulting SAR values from this study are higher than the ICNIRP exposure guidelines for occupational exposure in most cases except for the power density of 5 mW/cm². Besides the electric field intensity, the magnitude of dielectric and thermal properties in each tissue will directly affect the amount of SAR in the eye. For all power densities, the highest SAR values are obtained only in the region of the cornea, but not in lens and iris as electric field distributions. This is because the cornea has a much higher value of its dielectric properties (σ) than those of the lens and iris, as well as the cornea located close to the exposed surface, at which the electric field intensity is strongest. It is found that the SAR distribution pattern in the eye, which corresponds to Equation 22.14, strongly depends on the effect of the dielectric properties (σ , shown in Table 22.1) and thermal properties (ρ , shown in Table 22.2). With penetration into the eye, the SAR values decrease rapidly along the distance from the EM source.

22.4.4 Temperature Distribution

In order to study the heat transfer in the eye, the coupled effects of the EM wave propagation, the unsteady heat transfer, and the initial and boundary conditions are then investigated. Due to these effects, the electric field distribution (see Figure 22.6) and the SAR distribution (see Figure 22.7) are then converted into heat by absorption of the tissue.

22.4.4.1 Effect of Heat Transfer Model on Temperature Distribution

Since this study has focused on the volumetric heating effect into the multilayer tissues of the eye induced by EM fields, the effect of ambient temperature variation has been neglected in order to gain insight into the interaction between the EM fields and the human tissue as well as the correlation between the SAR and the heat transfer mechanism. For this reason, the ambient temperature has been set to the human body temperature of 37°C, and the tear evaporation has been neglected. Moreover, the effect of thermoregulation mechanisms has also been neglected due to the small temperature increase occurred during exposure process. The convective coefficient due to blood flow inside the sclera is set to 65 W/m² K [16].

For the eye exposed to the EM fields for a period of time, the temperature in the eye (Figure 22.8) is increased corresponding to the SAR (Figure 22.7). This is because the electric fields in the eye attenuate owing to the energy absorbed and thereafter the absorbed energy is converted to the thermal energy, which increases the eye temperature. Figure 22.8 shows the temperature distribution in the vertical cross section of the eye at various times exposed to the EM frequency of 900 MHz at the power density of 100 mW/cm² calculated using the conventional heat transfer model (Model I) (Figure 22.8a) and developed heat transfer model (Model II) (Figure 22.8b).

It is found that by using the different heat transfer models, the distribution patterns of temperature at a particular time are quite different. The hot spot zone is strongly displayed at 10 min for both heat transfer models at the anterior chamber area, owing to the extensive penetration of EM power of internal regions and higher dielectric properties (ϵ_r) of the anterior chamber tissue. This higher dielectric property of the anterior chamber represents the stronger absorption ability of EM fields than those of the cornea and lens. The outer corneal surface has a lower temperature than that of the anterior chamber, even if it has higher SAR value (Figure 22.7). This is because heat is dissipated to the ambient via convection and radiation since the main heat transfer mechanism of the conventional heat transfer model is the thermal conduction of the eye, whereas the developed heat transfer

AQ10

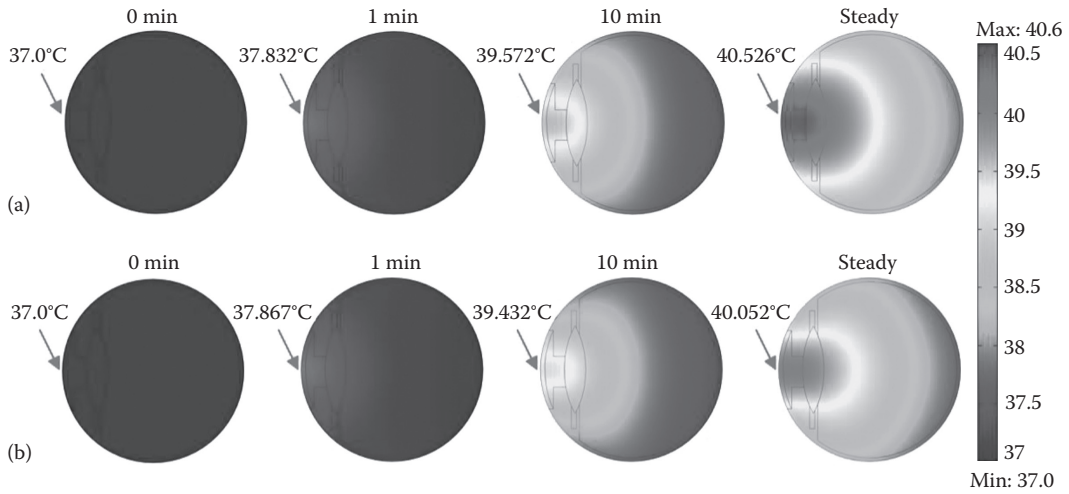


FIGURE 22.8

The temperature distribution in the human eye at various times exposed to the EM frequency of 900 MHz at the power density of 100 mW/cm² calculated using (a) the conventional heat transfer model and (b) the developed heat transfer model. (From Wessapan, T. and Rattanadecho, P., *ASME Trans. J. Heat Transfer*, 134, 091101, 2012. With permission.)

model accounts for the natural convection in the anterior chamber as well. Therefore, the developed heat transfer model with higher dissipation rates of heat generated by EM fields can obtain higher cooling effect than that of the conventional heat transfer model.

Consider the temperature increase distribution at the extrusion line (Figure 22.9). Figure 22.10 shows the temperature increase versus papillary axis (along the extrusion line) of the eye exposed to the EM frequency of 900 MHz at various times. In the early stage of

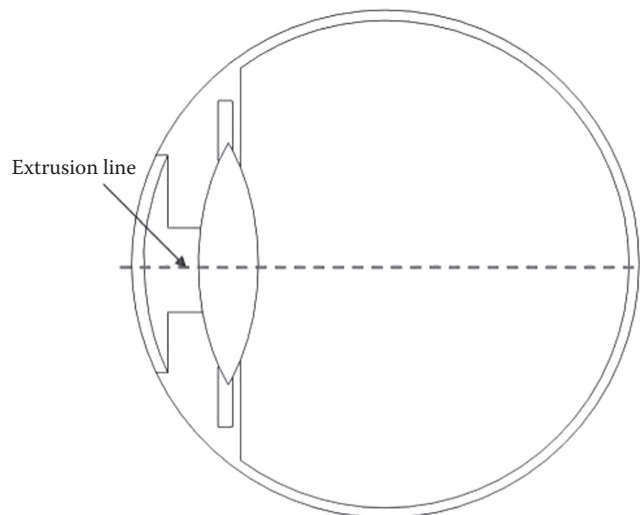


FIGURE 22.9

The extrusion line in the human eye where the temperature distribution is considered. (From Wessapan, T. and Rattanadecho, P., *ASME Trans. J. Heat Transfer*, 134, 091101, 2012. With permission.)

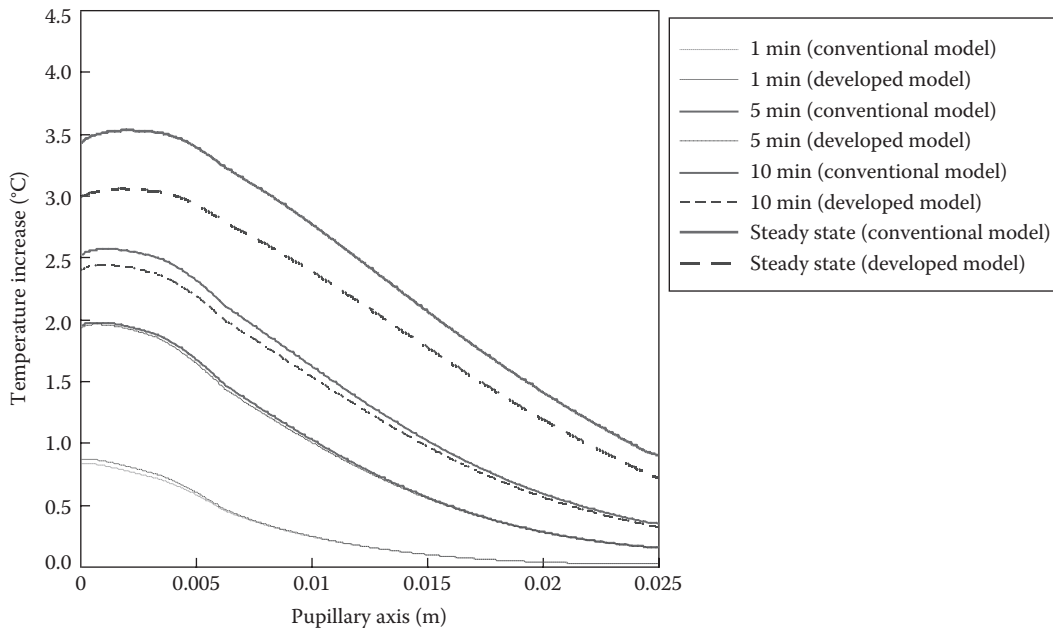


FIGURE 22.10

Temperature increase versus pupillary axis of the human eye exposed to the EM frequency of 900 MHz at various times. (From Wessapan, T. and Rattanadecho, P., *ASME Trans. J. Heat Transfer*, 134, 091101, 2012. With permission.)

exposure (1 min), the calculated temperature in the anterior chamber, obtained from the conventional heat transfer model, is little lower than that of developed heat transfer model. This is because natural convection in the developed heat transfer model causes a substantial accumulation of warmer fluid in the upper half of the anterior chamber. Surprisingly, just after 10 min of exposure, the temperature increase of the conventional heat transfer model is higher than that of developed heat transfer model. This is due to the presence of blood perfusion in the iris/sclera tissue, which covers an internal surface area of the eye. This blood perfusion provides buffer characteristic to the eye temperature, which is expected to occur in the realistic physiological conditions. Moreover, the natural convection and formation of two circulatory patterns with opposite direction in the anterior chamber, shown in Figure 22.11, play the important roles on the cooling processes in the eye, especially inner corneal surface, when a large temperature gradient is produced by EM fields after 10 min. The circulation pattern implies that the generated heat in the anterior chamber is convected in two directions: one is to the corneal surface and the other is to the lens surface.

22.4.4.2 Effect of Power Density on Temperature Distribution

In addition, each power density level is applied to investigate the effects of power density (the power irradiated on the eye surface). Figure 22.12 shows the comparison of the temperature distribution in the eye at time approaching to steady-state condition with the frequency of 900 MHz corresponding to the power densities of 5, 10, 50, and 100 mW/cm². It is found that the power densities significantly influence the temperature increase in the eye.

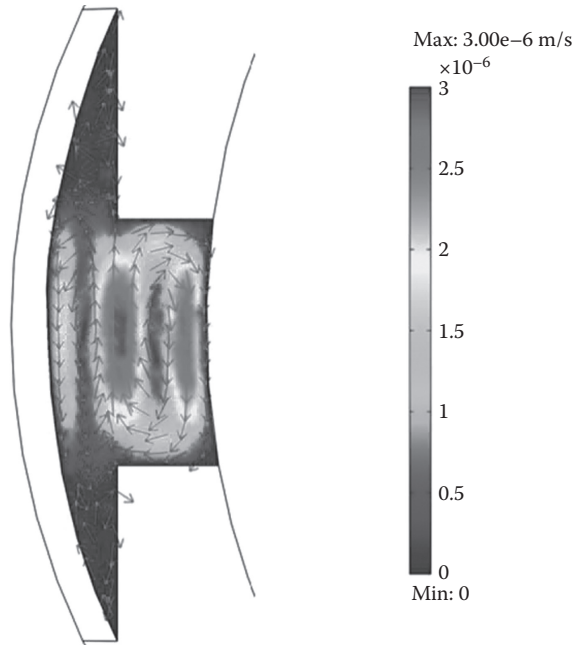


FIGURE 22.11 The velocity distribution inside the anterior chamber in the human eye when exposed to the EM frequency of 900 MHz. (From Wessapan, T. and Rattanadecho, P., *ASME Trans. J. Heat Transfer*, 134, 091101, 2012. With permission.)

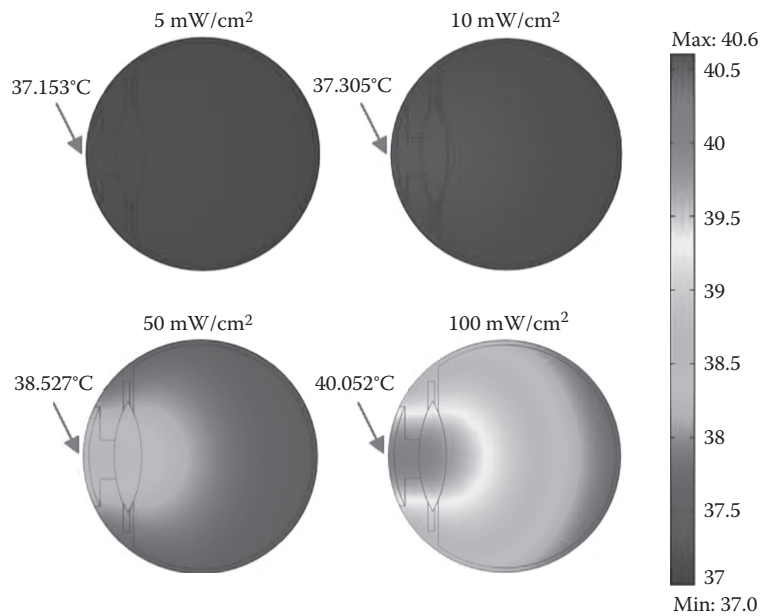
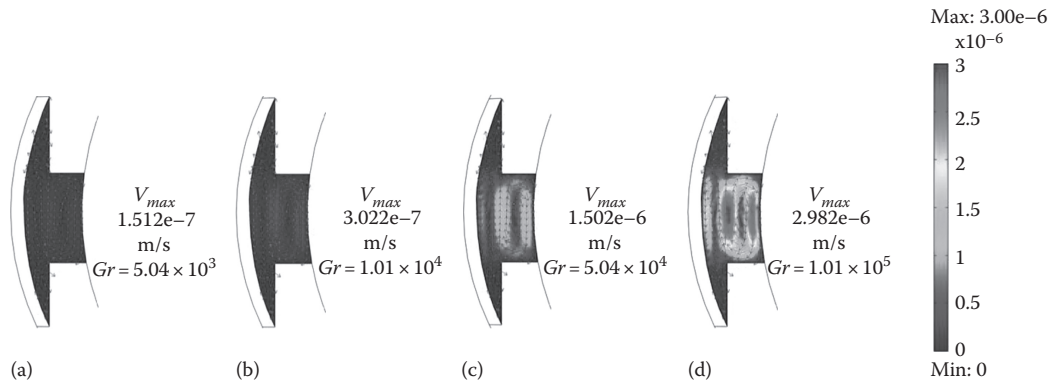


FIGURE 22.12 The temperature distribution in the eye exposed to the EM frequency of 900 MHz at various power densities calculated using (a) the conventional heat transfer model and (b) the developed heat transfer model. (From Wessapan, T. and Rattanadecho, P., *ASME Trans. J. Heat Transfer*, 134, 091101, 2012. With permission.)

**FIGURE 22.13**

The velocity distribution inside the anterior chamber in the eye exposed to the EM frequency of 900 MHz at the power densities of (a) 5 mW/cm², (b) 10 mW/cm², (c) 50 mW/cm², and (d) 100 mW/cm². (From Wessapan, T. and Rattanadecho, P., *ASME Trans. J. Heat Transfer*, 134, 091101, 2012. With permission.)

Greater power density provides greater heat generation inside the eye, thereby increasing the rate of temperature rise. By using the developed heat transfer model, the maximum temperature increases are 0.153°C, 0.305°C, 1.527°C, and 3.052°C at the power densities of 5, 10, 50, and 100 mW/cm², respectively.

Figure 22.13 shows the circulatory patterns in the anterior chamber in the eye exposed to the EM frequency of 900 MHz at various power densities. These circulatory patterns in the anterior chamber vary corresponding to the power densities that produced the temperature gradient in the eye. Therefore, in the case of a lower power density, the circulatory patterns have a lower speed, where a circulatory pattern with a higher power density flows faster. At the lower power density with low flow speed, the heat transfer in the anterior chamber occurs mainly by conduction across the fluid layer. In the case of the higher power density with higher flow speed, different flow regimes are encountered, with a progressively increasing heat transfer. The fluid motion within the anterior chamber is driven by the power density that is associated with the Grashof number Gr . The Grashof number is defined as $Gr = g\beta q D^5 / (k\nu^2)$, in which D is the eye diameter (m), q is the internal power density (W/m²), and ν is the kinematic viscosity (m²/s). The range of Grashof numbers investigated is 5.04×10^3 to 1.01×10^5 as shown in Figure 22.13.

22.4.5 Concluding Remarks

This study presents the numerical simulation of the SAR and temperature distributions in the eye exposed to TM mode of EM fields. The results of the SAR values in this study are increased corresponding to the electric field intensities. Besides the electric field intensity, the magnitude of dielectric and thermal properties in each tissue will directly affect the amount of SAR in the eye.

In this study, it is found that the highest level of SAR value is the cornea, while the highest temperature is the anterior chamber. In different heat transfer models, the temperature results obtained from a developed heat transfer model, considered natural convection and porous media theory, are compared to the results obtained from a conventional heat transfer model in order to highlight the advantages and the weakness of each model. It is found that by using the different heat transfer models, the distribution patterns of temperature

at a particular time are quite different. In all cases, the temperatures obtained from the developed heat transfer model have a lower temperature than that of the conventional heat transfer model. This is due to the presence of blood perfusion that provides buffer characteristic to the eye temperature, as well as the natural convection in the anterior chamber. It is found that greater power density results in a greater heat generation inside the eye, thereby increasing the rate of temperature increase. Moreover, it is found that the temperature distributions in the eye induced by EM fields are not directly related to the SAR distribution due to the effect of dielectric properties, thermal properties, blood perfusion, and penetration depth of the EM power.

The numerical simulations in this study show several important features of the energy absorption in the eye. This information can be used as a guideline for limiting human eye exposure from EM wave radiation.

References

1. Emery, A. F., Kramar, P., Guy, A. W., and Lin, J. C. 1975. Microwave induced temperature rises in rabbit eyes in cataract research. *J. Heat Transfer—T ASME* 97:123–128.
2. Buccella, C., Santis, V. D., and Feliaiani, M. 2007. Prediction of temperature increase in human eyes due to RF sources. *IEEE Trans. Electromagn. Compat.* 49:825–833.
3. Lin, J. C., 2003. Cataracts and cell-phone radiation. *IEEE Ant. Prop. Magazine* 45:171–174.
4. Fujiwara, O. and Kato, A. 1994. Computation of SAR inside eyeball for 1.5-GHz microwave exposure using finite-difference time domain technique. *IEICE Trans.* E77-B:732–737.
5. Gandhi, O. P., Lazzi, G., and Furse, C. M. 1996. Electromagnetic absorption in the human head and neck for mobile telephones at 835 and 1900 MHz. *IEEE Trans. Microw. Theory Tech.* 44:1884–1897.
6. International Commission on Non-Ionizing Radiation Protection (ICNIRP). 1998. Guidelines for limiting exposure to time-varying electric, magnetic and electromagnetic fields (up to 300 GHz). *Health Phys.* 74:494–522.
7. IEEE. 1999. IEEE standard for safety levels with respect to human exposure to radio frequency electromagnetic fields, 3 kHz to 300 GHz. IEEE Standard C95.1-1999.
8. Lagendijk, J. J. W. 1982. A mathematical model to calculate temperature distribution in human and rabbit eye during hyperthermic treatment. *Phys. Med. Biol.* 27:1301–1311.
9. Scott, J. 1988. A finite element model of heat transport in the human eye. *Phys. Med. Biol.* 33:227–241.
10. Scott, J. 1988. The computation of temperature rises in the human eye induced by infrared radiation. *Phys. Med. Biol.* 33:243–257.
11. Amara, E. H. 1995. Numerical investigations on thermal effects of Laser–Ocular media interaction. *Int. J. Heat Mass Transfer* 38:2479–2488.
12. Hirata, A., Matsuyama, S., and Shiozawa, T. 2000. Temperature rises in the human eye exposed to EM waves in the frequency range 0.6–6 GHz. *IEEE Trans. Electromagn. Compat.* 42:386–393.
13. Chua, K. J., Ho, J. C., Chou, S. K., and Islam, M. R. 2005. On the study of the temperature distribution within a human eye subjected to a laser source. *Int. Commun. Heat Mass Transfer* 32:1057–1065.
14. Limtrakarn, W., Reepolmaha, S., and Dechaumphai, P. 2010. Transient temperature distribution on the corneal endothelium during ophthalmic phacoemulsification: A numerical simulation using the nodeless variable element. *Asian Biomed.* 4:885–892.
15. Kumar, S., Acharya, S., Beuerman, R., and Palkama, A. 2006. Numerical solution of ocular fluid dynamics in a rabbit eye: Parametric effects. *Ann. Biomed. Eng.* 34:530–544.

16. Ooi, E. and Ng, E. Y. K. 2008. Simulation of aqueous humor hydrodynamics in human eye heat transfer. *Comput. Biol. Med.* 38:252–262.
17. Ooi, E. H. and Ng, E. Y. K. 2011. Effects of natural convection inside the anterior chamber. *Int. J. Numer. Methods Biomed. Eng.* 27: 408–423.
18. Pennes, H. H. 1948. Analysis of tissue and arterial blood temperatures in the resting human forearm. *J. Appl. Physiol.* 1:93–122.
19. Pennes, H. H. 1998. Analysis of tissue and arterial blood temperatures in the resting human forearm. *J. Appl. Physiol.* 85:5–34.
20. Flyckt, V. M. M., Raaymakers, B. W., and Lagendijk, J. J. W. 2006. Modeling the impact of blood flow on the temperature distribution in the human eye and the orbit: Fixed heat transfer coefficients versus the pennes bioheat model versus discrete blood vessels. *Phys. Med. Biol.* 51:5007–5021.
21. Ng, E. Y. K. and Ooi, E. H. 2006. FEM simulation of the eye structure with bioheat analysis. *Comput. Methods Programs Biomed.* 82:268–276.
22. Ooi, E. H. and Ng, E. Y. K. 2006. Ocular temperature distribution: A mathematical perspective. *J. Mech. Med. Biol.* 9:199–227.
23. Nakayama, A. and Kuwahara, F. 2008. A general bioheat transfer model based on the theory of porous media. *Int. J. Heat Mass Transfer* 51:3190–3199.
24. Mahjoob, S. and Vafai, K. 2009. Analytical characterization of heat transfer through biological media incorporating hyperthermia treatment. *Int. J. Heat Mass Transfer* 52:1608–1618.
25. Khanafer, K. and Vafai, K. 2009. Synthesis of mathematical models representing bioheat transport. In *Advances in Numerical Heat Transfer*, eds. W. J. Minkowycz, E. M. Sparrow, and J. P. Abraham, pp. 1–28. London, U.K.: Taylor & Francis.
26. Shafahi, M. and Vafai, K. 2011. Human eye response to thermal disturbances. *J. Heat Transfer—T ASME* 133:011009.
27. Narasimhan, A. and Vishnampet, R. 2012. Effect of choroidal blood flow on transscleral retinal drug delivery using a porous medium model. *Int. J. Heat Mass Transfer* 55:5665–5672.
28. Kumarjha, K. and Narasimhan, A. 2011. Three-dimensional bio-heat transfer simulation of sequential and simultaneous retinal laser irradiation. *Int. J. Thermal Sci.* 50:1191–1198.
29. Narasimhan, A. and Sadasivam, S. 2013. Non-Fourier bio heat transfer modelling of thermal damage during retinal laser irradiation. *Int. J. Heat Mass Transfer* 60:591–597.
30. Ooi, E. H., Ang, W. T., and Ng, E. Y. K. 2008. A boundary element model of the human eye undergoing laser thermokeratoplasty. *Comput. Biol. Med.* 28:727–738.
31. Ooi, E. H., Ang, W. T., and Ng, E. Y. K. 2008. A boundary element model for investigating the effects of eye tumor on the temperature distribution inside the human eye. *Comput. Biol. Med.* 39:667–677.
32. Tan, J. H., Ng, E. Y. K., and Acharya, U. R. 2011. Evaluation of topographical variation in ocular surface temperature by functional infrared thermography. *Infrared Phys. Technol.* 54:469–477.
33. Tan, J. H., Ng, E. Y. K., and Acharya, U. R. 2010. Evaluation of tear evaporation from ocular surface by functional infrared thermography. *Med. Phys.* 37:6022–6034.
34. Tan, J. H., Ng, E. Y. K., Acharya, U. R., and Chee, C. Study of normal ocular thermogram using textural parameters. *Infrared Phys. Technol.* 53:120–126.
35. Wessapan, T. and Rattanadecho, P. Specific absorption rate and temperature increase in human eye subjected to electromagnetic fields at 900 MHz. *ASME Trans. J. Heat Transfer* 134:091101.
36. Bernardi, P., Cavagnaro, M., Pisa, S., and Piuze, E. 2000. Specific absorption rate and temperature increases in the head of a cellular-phone user. *IEEE Trans. Microw. Theory Tech.* 48:1118–1126.
37. Park, S., Jeong, J., and Lim, Y. 2004. Temperature rise in the human head and brain for portable handsets at 900 and 1800 MHz. *4th International Conference on Microwave and Millimeter Wave Technology, ICMMT 2004, Beijing, China.* AQ11
38. Nakayama, A. and Kuwahara, F. 2008. A general bioheat transfer model based on the theory of porous media. *Int. J. Heat Mass Transfer* 51:3190–3199.

AUTHOR QUERIES

- [AQ1] Please check if edit to the sentence starting "Since the eye..." is okay.
- [AQ2] Please check if edit to the sentence starting "For example, in..." is okay.
- [AQ3] Please check the caption of Figures 22.1 through 22.13 for correctness.
- [AQ4] " σ " is not provided in Equation 22.13. Please check.
- [AQ5] Please check if edit to the sentence starting "According to the..." is okay.
- [AQ6] " \bar{E}_i " is not mentioned in Equation 22.14. Please check.
- [AQ7] Please check if edit to the sentence starting "The energy equation..." is okay.
- [AQ8] Please check if edit to the sentence starting "This is because..." is okay.
- [AQ9] Please check if edit to the sentence starting "The results of..." is okay.
- [AQ10] Please check if edit to the sentence starting "This is because..." is okay.
- [AQ11] Please check the conference title and location for Ref. [37].